Rapid and Quantitative Activation of *Chlamydia trachomatis* Ribonucleotide Reductase by Hydrogen Peroxide†

Wei Jiang,‡ Jiajia Xie,‡ Hanne Nørgaard,‡ J. Martin Bollinger, Jr.,*,‡,§ and Carsten Krebs*,‡,§

Department of Biochemistry and Molecular Biology and Department of Chemistry, The Pennsylvania State University, University Park, Pennsylvania 16802

Received October 16, 2007; Revised Manuscript Received January 24, 2008

ABSTRACT: We recently showed that the class Ic ribonucleotide reductase (RNR) from the human pathogen *Chlamydia trachomatis* (*Ct*) uses a Mn^{IV}/Fe^{III} cofactor in its R2 subunit to initiate catalysis [Jiang, W., Yun, D., Saleh, L., Barr, E. W., Xing, G., Hoffart, L. M., Maslak, M.-A., Krebs, C., and Bollinger, J. M., Jr. (2007) *Science 316*, 1188–1191]. The Mn^{IV} site of the novel cofactor functionally replaces the tyrosyl radical used by conventional class I RNRs to initiate substrate radical production. As a first step in evaluating the hypothesis that the use of the alternative cofactor could make the RNR more robust to reactive oxygen and nitrogen species [RO(N)S] produced by the host's immune system [Högbom, M., Stenmark, P., Voevodskaya, N., McClarty, G., Gräslund, A., and Nordlund, P. (2004) *Science 305*, 245–248], we have examined the reactivities of three stable redox states of the Mn/Fe cluster (Mn^{II}/Fe^{II}, Mn^{III}/Fe^{III}, and Mn^{IV}/Fe^{III}) toward hydrogen peroxide. Not only is the activity of the Mn^{IV}/Fe^{III}−R2 intermediate stable to prolonged (>1 h) incubations with as much as 5 mM H_2O_2, but both the fully reduced (Mn^{II}/Fe^{II}) and one-electron-reduced (Mn^{III}/Fe^{III}) forms of the protein are also efficiently activated by H_2O_2. The Mn^{III}/Fe^{III}−R2 species reacts with a second-order rate constant of 8 ± 1 M^{-1} s^{-1} to yield the Mn^{IV}/Fe^{IV}−R2 intermediate previously observed in the reaction of Mn^{II}/Fe^{II}−R2 with O_2 [Jiang, W., Hoffart, L. M., Krebs, C., and Bollinger, J. M., Jr. (2007) *Biochemistry 46*, 8709–8716]. As previously observed, the intermediate decays by reduction of the Fe site to the active Mn^{IV}/Fe^{III}−R2 complex. The reaction of the Mn^{II}/Fe^{II}−R2 species with H_2O_2 proceeds in three resolved steps: sequential oxidation to Mn^{III}/Fe^{III}−R2 ($k = 1.7 \pm 0.3$ mM^{-1} s^{-1}) and Mn^{IV}/Fe^{IV}−R2, followed by decay of the intermediate to the active Mn^{IV}/Fe^{III}−R2 product. The efficient reaction of both reduced forms with H_2O_2 contrasts with previous observations on the conventional class I RNR from *Escherichia coli*, which is efficiently converted from the fully reduced ($Fe_2^{II/II}$) to the "met" ($Fe_2^{III/III}$) form [Gerez, C., and Fontecave, M. (1992) *Biochemistry 31*, 780–786] but is then only very inefficiently converted from the met to the active ($Fe_2^{III/III}$−$Y^{\bullet}$) form [Sahlin, M., Sjöberg, B.-M., Backes, G., Loehr, T., and Sanders-Loehr, J. (1990) *Biochem. Biophys. Res. Commun. 167*, 813–818].

Ribonucleotide reductases (RNRs)[1] catalyze the reduction of ribonucleotides to 2′-deoxyribonucleotides to provide precursors for DNA synthesis and repair. A conventional class I RNR, such as that from *Escherichia coli* (*Ec*) or *Homo sapiens*, harbors in its R2 subunit a cofactor comprising a tyrosyl radical ($Y^{\bullet}$) and an adjacent carboxylate-bridged $Fe_2^{III/III}$ cluster (*1*). The cofactor components form together by reaction of O_2 with the fully reduced ($Fe_2^{II/II}$) form of the cluster (*1*). A $Fe_2^{III/IV}$ intermediate, **X**, oxidizes the tyrosine residue to the stable $Y^{\bullet}$ as it is reduced to the product $Fe_2^{III/III}$ cluster (*2–4*). In the catalytic cycle, the $Y^{\bullet}$ in R2 oxidizes a cysteine residue in the R1 subunit by a long-distance (∼35 Å), intersubunit, proton-coupled electron transfer (PCET), generating a transient cysteine thiyl radical (*5, 6*). The cysteine radical in R1 initiates reduction of the ribonucleoside diphosphate (NDP) substrate by abstracting the hydrogen atom from C3′ (*7, 8*). After reduction of the substrate 3′ radical to the product 3′ radical by two additional cysteine residues in R1 (which become oxidized to a disulfide), the hydrogen originally abstracted from C3′ is returned to this position, regenerating the cysteine radical and yielding the dNDP product. The cysteine radical then reoxidizes the Y in R2 to the stable $Y^{\bullet}$.

Inhibition of RNRs is a proven strategy for combating cancer and some viruses (*9–11*). Reduction of the catalytically essential $Y^{\bullet}$ in R2 is part of the mechanisms of action of several RNR-targeting drugs (*12–14*). For example, the anticancer drug hydroxyurea reduces the $Y^{\bullet}$ to tyrosine (*15, 16*),

† This work was supported by the National Institutes of Health (Grant GM-55365 to J.M.B.), the Beckman Foundation (Young Investigator Award to C.K.), and the Dreyfus Foundation (Teacher Scholar Award to C.K.).

* To whom correspondence should be addressed. J.M.B.: Department of Biochemistry and Molecular Biology, 208 Althouse Laboratory, University Park, PA 16802; phone, (814) 863-5707; fax, (814) 863-7024; e-mail, jmb21@psu.edu. C.K.: Department of Biochemistry and Molecular Biology, 306 South Frear Laboratory, University Park, PA 16802; phone, (814) 865-6089; fax, (814) 863-7024; e-mail, ckrebs@psu.edu.

‡ Department of Biochemistry and Molecular Biology.

§ Department of Chemistry.

[1] Abbreviations: RNR, ribonucleotide reductase; NDP, nucleoside diphosphate; dNDP, 2′-deoxynucleoside diphosphate; *Ct*, *Chlamydia trachomatis*; *Ec*, *Escherichia coli*; DTT, dithiothreitol; EPR, electron paramagnetic resonance; EDTA, ethylenediaminetetraacetate; RO(N)S, reactive oxygen/nitrogen species; $Y^{\bullet}$, tyrosyl radical.

10.1021/bi702085z CCC: $40.75
Published on Web 03/22/2008

yielding a state known as met-R2. Adventitious reduction of the potently oxidizing Y• to give met-R2 may also occur in the reducing environment of the cell. An enzymatic reactivating system capable of slowly (over many minutes) regenerating the Y• by mediating reduction of the $Fe_2^{III/III}$ cluster in *Ec* met-R2 to $Fe_2^{II/II}$ (which then reacts with O_2) was reported and studied by Reichard, Fontecave, and co-workers (*17, 18*), but its physiological relevance has not been established. More recently, Stubbe and co-workers identified a [2Fe-2S] cluster-containing ferredoxin, YfaE, that can reduce *Ec* met-R2 rapidly (in seconds) to the $Fe_2^{II/II}$ form, leading to rapid formation of Y• upon exposure to O_2 (*19*). This reaction is likely to be relevant to control of the Y• content of R2 *in vivo*. *In vitro* reactivation of met-R2 by H_2O_2 has also been reported, but this reaction is very inefficient (regeneration of 30% of the Y• in 1.5 h) (*20*).

When McClarty and co-workers identified the genes encoding the class I RNR subunits from several species of chlamydiae, they noted that the R2 proteins have phenylalanine (F) residues aligning with the radical-harboring tyrosines of the other R2 proteins (*21*). They found that the R2 from *Ct* is, nevertheless, catalytically active (*21*). Subsequent biochemical and structural characterization of *Ct* R2 by Nordlund, Gräslund, and co-workers confirmed the absence of the Y• and the location of F at the corresponding site, and a new subclass (Ic) was established to comprise the *Ct* enzyme and the hypothetical Y•-less RNRs encoded within the genomes of several other bacteria and archaea (*22*). In that same study and in two subsequent reports from the Gräslund group, the hypothesis was advanced that reaction of O_2 with the $Fe_2^{II/II}$ cluster generates a high-valent $Fe_2^{III/IV}$ cofactor (similar to the Y•-generating cluster **X** in the conventional R2 proteins) that functionally replaces the Y• as the radical initiator in the class Ic RNRs (*22–24*). It was further speculated in the case of the *Ct* RNR that the use of the novel cofactor might render the RNR and bacterium (an obligate intracellular parasite) more robust to reactive oxygen and nitrogen species [RO(N)S] produced in the host's innate immune response (*22*). Indeed, several earlier studies had shown that the Y• in the conventional class I system can be targeted by RO(N)S (*25–30*).

We recently verified an essential aspect of the Nordlund−Gräslund hypothesis, the functional replacement of the Y• with a high-valent metal cofactor, but showed that the *Ct* R2 actually uses a heterobinuclear Mn^{IV}/Fe^{III} cofactor (*31, 32*), rather than the homobinuclear $Fe_2^{III/IV}$ cofactor proposed by these authors, as the radical initiator. The functional cofactor forms via a Mn^{IV}/Fe^{IV} intermediate in the reaction of the Mn^{II}/Fe^{II} form of the protein with O_2 (*33*). The Mn^{IV} ion replaces the Y• of the conventional class I RNRs as the radical initiator (*31*). This "metal makeover" (*34*) does not rule out the second aspect of the Nordlund−Gräslund hypothesis, that the alternative radical initiation system renders the enzyme more resistant to host-generated RO(N)S. In fact, in light of the several precedents for the involvement of Mn in bacterial oxidative stress responses (*35–37*), its presence in the *Ct* RNR cofactor would seem to make this hypothesis even more attractive. In this work, we have begun to test the second aspect of the Nordlund−Gräslund hypothesis by examining the reactivity of the Mn/Fe cofactor toward H_2O_2, a biologically important RO(N)S. Among the biologically important RO(N)S, hydrogen peroxide is the most stable and its chemistry the most simple. Moreover, its production is known to be an important component of innate immunity to bacteria (*38*). The complete stability of the active Mn^{IV}/Fe^{III}−R2 species and rapid, quantitative conversion of both fully reduced (Mn^{II}/Fe^{II}) and one-electron-reduced (Mn^{III}/Fe^{III}) forms of the protein to the active state upon their treatment with H_2O_2, when contrasted with previous observations on the reactions of fully reduced (*39, 40*) and met forms (*20*) of *Ec* R2 with H_2O_2, are consistent with the hypothesis that the novel radical initiation system could be an adaptation to RO(N)S produced by the host.

MATERIALS AND METHODS

Expression and Purification of Ct R2. Ct R2 with an N-terminal 22-residue extension containing a His_6 affinity tag was expressed in *E. coli*, purified by chromatography on Ni-NTA agarose, and converted to the metal-free (apo) form as previously described (*31*).

Preparation of the Mn^{IV}/Fe^{III}−R2 Species. To an air-saturated solution of 370 μM (monomer concentration) apo R2 at 5 °C were added 1.5 equiv of Mn^{II} and 5 mM sodium ascorbate. Fe^{II} (0.75 equiv per monomer of either natural abundance or ∼95% ^{57}Fe-enriched Fe^{II}) was added slowly over a period of 20 min. After 1 h at 5 °C, unbound metal was removed by dialysis against 10 mM EDTA [in 100 mM Na-HEPES (pH 7.6) and 10% glycerol]. The EDTA was removed from the protein by dialysis against buffer [100 mM Na-HEPES (pH 7.6) and 10% glycerol]. Removal of >95% of the free Mn^{II} was verified by EPR spectroscopy. Mössbauer analysis of ^{57}Fe-labeled samples indicated the presence of 85–90% of the active Mn^{IV}/Fe^{III} form and 10–15% of the inactive $Fe_2^{III/III}$ form.

Preparation of the Mn^{III}/Fe^{III}−R2 Species. The Mn^{IV}/Fe^{III}−R2 form was reduced in an MBraun anoxic chamber with 1.2 molar equiv (2.4 electron equiv) of sodium dithionite for 60 min and subsequently used for the kinetic and spectroscopic experiments. The Mn^{III}/Fe^{III}−R2 species used for the activity assays was prepared by treatment of the active protein with 7.5 molar equiv of sodium dithionite to completely eliminate activity. EPR spectroscopy showed that >80% of the protein was converted to the one-electron-reduced Mn^{III}/Fe^{III} state (i.e., that <20% was further reduced by the excess dithionite).

Activity Assays. The enzymatic activity supported by samples of *Ct* R2 in the presence of excess R1, CDP, ATP, and DTT was determined as previously described (*31*).

Kinetic and Spectroscopic Experiments. The stopped-flow apparatus, the EPR and Mössbauer spectrometers, and the freeze-quench apparatus and procedures have been described previously (*41*). Absorbance-versus-time traces from the reactions of Mn^{III}/Fe^{III}−R2 and Mn^{II}/Fe^{II}−R2 species with H_2O_2 were analyzed by nonlinear regression according to eqs 1 and 2, respectively, in which k_1−k_3 are apparent first-order rate constants, ΔA_1−ΔA_3 are amplitudes for the exponential phases, and A_0 is the absorbance at time zero. The assumption of a pseudo-first-order excess of H_2O_2 inherent in these equations is met by the experimental conditions. The assumption of irreversibility is reasonable because cleavage of H_2O_2 to water is highly exergonic.

$$A(t) = A_0 + \Delta A_1[1 - \exp(-k_1 t)] + \Delta A_2[1 - \exp(-k_2 t)] \quad (1)$$

$$A(t) = A_0 + \Delta A_1[1 - \exp(-k_1 t)] + \Delta A_2[1 - \exp(-k_2 t)] + \Delta A_3[1 - \exp(-k_3 t)] \quad (2)$$

Colorimetric Assay for H_2O_2 Concentration. All H_2O_2 concentrations quoted were calculated by assuming the concentration listed on the commercially obtained stock solution (EMD, Gibbstown, NJ). This concentration was verified by using a previously described colorimetric assay (*42*). The experimentally determined H_2O_2 concentration (8.3 mM) agreed with the value quoted by the manufacturer (8.8 mM). The same assay was also used to monitor decomposition of H_2O_2 in the presence of various forms of *Ct* R2.

RESULTS

H_2O_2 Does Not Inactivate the Mn^{IV}/Fe^{III}−R2 Complex. Incubation of the active Mn^{IV}/Fe^{III}−R2 complex with as much as 5 mM H_2O_2 for as long as 60 min before the protein is used to initiate the activity assay does not result in a detectable loss of activity.

H_2O_2 Reactivates the Mn^{III}/Fe^{III}−R2 Complex Prepared by Dithionite Reduction of the Active Form. Treatment of the Mn^{IV}/Fe^{III}−R2 complex with 7.5 molar equiv of dithionite per R2 monomer as described in Materials and Methods diminishes the activity to undetectable levels (v/[R2] < 0.02 s^{-1}). Subsequent treatment with H_2O_2 for 10 min restores activity (Table 1). Under these conditions, 10 molar equiv of H_2O_2 is required to maximally reactivate. The activity is then not significantly different from the activity of the Mn^{IV}/Fe^{III}−R2 complex before its reduction with dithionite. Upon addition of excess H_2O_2 (100 mM) to the inactive Mn^{III}/Fe^{III}−R2 complex, quantitative reactivation is complete in less than 5 min (data not shown).

Characterization of H_2O_2-Mediated Reactivation by Mössbauer Spectroscopy. The activity assays demonstrate rapid and quantitative reactivation of dithionite-reduced (Mn^{III}/Fe^{III}) *Ct* R2 by H_2O_2. Mössbauer spectroscopy was used to verify that this reactivation reflects conversion of the inactive Mn^{III}/Fe^{III}−R2 form to the active Mn^{IV}/Fe^{III} form. First, the Mn^{IV}/Fe^{III}−R2 complex to be converted by dithionite treatment to the Mn^{III}/Fe^{III}−R2 complex was characterized (Figure 1A). The Mn^{IV}/Fe^{III}−R2 species exhibits a sharp quadrupole doublet at 4.2 K and zero field. Figure 1A shows that, in this particular sample of the Mn^{IV}/Fe^{III}−R2 complex, approximately 90% of the iron is in the form of the Mn^{IV}/Fe^{III} cluster. Its quadrupole doublet has an isomer shift (δ) of 0.52 mm/s and a quadrupole splitting parameter (ΔE_Q) of 1.38 mm/s (solid line in Figure 1A). ΔE_Q is slightly larger than the value reported previously [ΔE_Q = 1.32 mm/s (*32*)]. We attribute this to the presence of a greater concentration of glycerol in this sample (45%, v/v) than in the previous sample (10%, v/v). The sample also contains a minor (~10%) contaminant of the homobinuclear $Fe_2^{III/III}$ complex (red line). At 190 K and zero field (Figure 1B), the isomer shift of the Fe^{III} site is slightly diminished (δ = 0.47 mm/s) by the second-order Doppler effect (*43*). The quadrupole splitting is temperature-independent (ΔE_Q = 1.37 mm/s) and identical within the experimental uncertainty (0.03 mm/s) to the value at 4.2 K.

Treatment of this sample with 1.2 equiv of dithionite alters the 190 K/zero field spectrum (Figure 1C) to a much broader quadrupole doublet with parameters (δ = 0.45 mm/s, ΔE_Q = 0.83 mm/s) still characteristic of high-spin Fe^{III} (*43*), implying [as previously noted (*31*)] that the Fe site of the cofactor is not reduced. The 4.2 K/53 mT spectrum of the reduced sample is broad and magnetically split (Figure S1). These observations are consistent with reduction of the Mn^{IV} site to yield a Mn^{III}/Fe^{III} cluster with an $S = {}^1/_2$ ground state, as previously reported (*31*).

The Mössbauer spectra of this sample after its subsequent treatment with excess H_2O_2 (300 mM or 100 equiv for 15 min) confirm the essentially quantitative conversion of the dithionite-inactivated (Mn^{III}/Fe^{III}) R2 back to the active Mn^{IV}/Fe^{III} state (Figure 1D,E). The spectra are identical within the experimental uncertainty to those of the Mn^{IV}/Fe^{III}−R2 sample prior to its reduction with dithionite (Figure 1A,B).

Table 1: Relative Activity of *C. trachomatis* RNR upon Treatment of the R2 Protein with H_2O_2

	equiv of H_2O_2	activity (%)
Mn^{III}/Fe^{III}	0	<5
	2.5	19 ± 9
	5	48 ± 29
	10	83 ± 28
	20	93 ± 21
	50	90 ± 23
Mn^{IV}/Fe^{III}	−	100[a]

[a] The activity of the Mn^{IV}/Fe^{III}−R2 complex is ~0.4 s^{-1} or 600 units/mg under the assay conditions that were used (22 ± 2 °C, 10 equiv of R1).

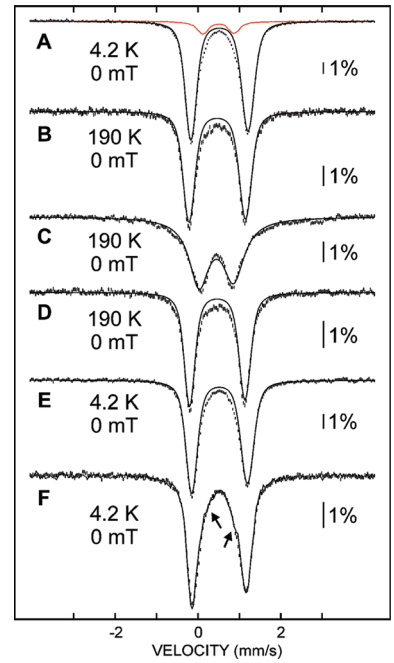

FIGURE 1: Mössbauer spectra showing the reduction of the Mn^{IV}/Fe^{III}−R2 complex to the Mn^{III}/Fe^{III}−R2 complex by dithionite and reoxidation to the Mn^{IV}/Fe^{III}−R2 complex by H_2O_2. The temperature and magnetic field are indicated on the spectra. (A and B) A sample of the Mn^{IV}/Fe^{III}−R2 complex prepared as described in Materials and Methods. (C) A sample after treatment of the Mn^{IV}/Fe^{III}−R2 complex with 1.2 equiv of dithionite for 1 h. (D and E) Dithionite-reduced sample after subsequent treatment with 300 mM H_2O_2 for 15 min. (F) Samples prepared by exposure of the Mn^{II}/Fe^{II}−R2 complex (1.5 mM R2 monomer, 1 equiv of Mn^{II}, and 0.5 equiv of Fe^{II}) to 300 mM H_2O_2 (hash marks) or 1 mM O_2 (solid line). The solid black lines plotted over spectra A−E are simulations with parameters quoted in the text. The red line is the experimental spectrum of the $Fe_2^{III/III}$−R2 form, scaled to 10% of the total intensity of spectrum A.

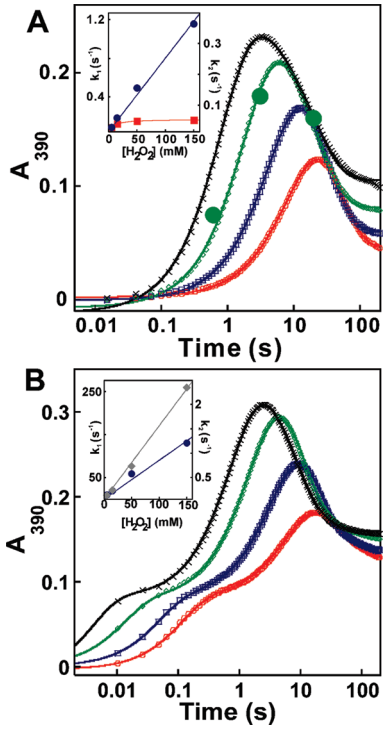

FIGURE 2: Kinetics of the reactions of the (A) Mn^{III}/Fe^{III}−R2 and (B) Mn^{II}/Fe^{II}−R2 complexes with excess H_2O_2. The final H_2O_2 concentrations are 5 (red), 15 (blue), 50 (green), and 150 mM (black). (A) A sample of the Mn^{III}/Fe^{III}−R2 complex (0.40 mM R2 monomer, 0.75 equiv of Fe, and 0.75 equiv of Mn), prepared as described in Materials and Methods by dithionite reduction of the Mn^{IV}/Fe^{III}−R2 complex, was mixed at 5 °C with an equal volume of an H_2O_2 solution in the same buffer. The green circles are the EPR signal intensities from the experiment of Figure 3 scaled for direct comparison to the absorbance changes. The solid lines are fits according to eq 1. The inset shows the apparent first-order rate constants ($k_{obs,1}$ and $k_{obs,2}$) for the formation and decay phases (blue circles and red squares, respectively) vs H_2O_2 concentration, which gives a second-order rate constant (slope) of 8 ± 1 M^{-1} s^{-1} for formation and a limiting rate constant of 0.06 ± 0.01 s^{-1} for decay. (B) A solution of the Mn^{II}/Fe^{II}−R2 complex (0.40 mM R2 monomer, 0.5 equiv of Fe^{II}, and 1.5 equiv of Mn^{II}) was mixed at 5 °C with an equal volume of an H_2O_2 solution. The solid lines are fits according to eq 2. The inset shows k_{obs} values for the two formation phases of the reaction vs H_2O_2 concentration. The plot gives second-order rate constants of 1.7 ± 0.3 mM^{-1} s^{-1} for the first phase (gray diamonds) and 8 ± 1 M^{-1} s^{-1} for the second phase (blue circles).

As the solid lines in D and E indicate, ~90% of the intensity can again be attributed to the quadrupole doublet of the Mn^{IV}/Fe^{III}−R2 complex [$\delta = 0.47$ mm/s and $\Delta E_Q = 1.34$ mm/s at 190 K (D), and $\delta = 0.52$ mm/s and $\Delta E_Q = 1.35$ mm/s at 4.2 K (E)].

Kinetics and Mechanisms of the Reaction of the Mn^{III}/Fe^{III}−R2 Complex with H_2O_2 by Stopped-Flow Absorption and Freeze-Quench EPR Spectroscopies. Stopped-flow absorption and freeze-quench EPR experiments were used to define the kinetics and mechanism of H_2O_2-mediated reactivation of the dithionite-generated Mn^{III}/Fe^{III}−R2 complex. An intense ~390 nm absorption band, similar to the feature associated with the Mn^{IV}/Fe^{IV}−R2 intermediate in the reaction of the fully reduced (Mn^{II}/Fe^{II}) protein with O_2 (*33*), develops rapidly upon mixing of the Mn^{III}/Fe^{III}−R2 complex with H_2O_2 and then decays slowly (Figure S2). Analysis of A_{390}-versus-time traces for the reaction (Figure 2A) according to eq 1 reveals that the formation phase has the expected

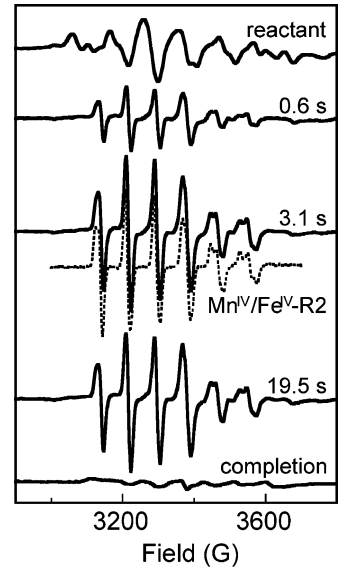

FIGURE 3: X-Band EPR spectra at 14.0 ± 0.2 K of freeze-quenched samples from the reaction between the Mn^{III}/Fe^{III}−R2 complex and 50 mM H_2O_2. The reaction was initiated by mixing the Mn^{III}/Fe^{III}−R2 sample (0.90 mM R2 monomer and 0.75 equiv of each metal) with 0.5 equivalent volume of 150 mM H_2O_2, and samples were rapidly frozen at the indicated reaction times. For the spectra of the three freeze-quenched samples that are shown (indicated by reaction time), the spectrum of the reactant sample was scaled appropriately and then subtracted from the experimental spectrum of each sample to resolve the contribution of the Mn^{IV}/Fe^{IV}−R2 intermediate. The dashed spectrum, taken from ref *33*, is that of the Mn^{IV}/Fe^{IV}−R2 intermediate in the reaction of the Mn^{II}/Fe^{II}−R2 complex with O_2. Spectrometer conditions were as follows: microwave frequency, 9.45 GHz; microwave power, 200 μW; modulation frequency, 100 kHz; modulation amplitude, 10 G; scan time, 167 s; time constant, 167 ms.

first-order dependence on H_2O_2 concentration, whereas the decay phase is relatively insensitive to H_2O_2 concentration (inset of Figure 2A). The slope of the plot of the apparent first-order rate constant for the formation phase (k_{obs}) versus H_2O_2 concentration [inset of Figure 2A (circles)] gives a second-order rate constant of 8 ± 1 M^{-1} s^{-1} for the reaction of the Mn^{III}/Fe^{III}−R2 complex with H_2O_2. The kinetics of the decay phase (limiting $k_{obs} = 0.06 \pm 0.01$ s^{-1}) are consistent with those previously observed for decay of the Mn^{IV}/Fe^{IV} complex to Mn^{IV}/Fe^{III}−R2 complex (*33*). Thus, both the character of the spectral changes and the kinetics suggest the accumulation of the Mn^{IV}/Fe^{IV}−R2 intermediate.

The accumulation of this complex was directly demonstrated by freeze-quench EPR experiments (Figure 3). The dithionite-reduced R2 reactant exhibits a broad, poorly defined $g \sim 2$ EPR spectrum (top spectrum) from the antiferromagnetically coupled ($S = {}^1/_2$) Mn^{III}/Fe^{III} cluster.[2] When this reactant is mixed with H_2O_2, the well-defined, sharp, six-line signal characteristic of the Mn^{IV}/Fe^{IV}−R2 intermediate [dashed spectrum (*33*)] develops rapidly and then slowly decays. The kinetics of the intermediate obtained from the intensity of the EPR signal at different reaction times (green circles in Figure 2A) agree well with the A_{390}-versus-time trace from the stopped-flow experiment with the same H_2O_2 concentration.

[2] We have seen marked variability in the shape of this signal. In particular, it varies considerably with the Mn/R2 stoichiometry and the details of how the protein has been reconstituted prior to reduction. We are investigating the structural basis for this variability.

Activation of the Fully Reduced Mn^{II}/Fe^{II}−R2 Complex with H_2O_2. Previous studies have shown that the fully reduced ($Fe_2^{II/II}$) form of *Ec* R2 reacts with H_2O_2 to produce met-R2 (*39, 40*). The cognate reaction in *Ct* R2 would convert the Mn^{II}/Fe^{II} complex to the Mn^{III}/Fe^{III}−R2 complex, which should, as demonstrated above, then react with a second equivalent of H_2O_2 to yield the active state. Indeed, treatment of the Mn^{II}/Fe^{II}−R2 complex with excess H_2O_2 results in an activity equivalent to that produced by treatment with O_2. In addition, the 4.2 K/zero field Mössbauer spectra (Figure 1F) of the products of the H_2O_2 (hash marks) and O_2 (solid line) reactions are nearly identical.[3] In both cases, application of the 53 mT magnetic field elicits the same diagnostic broadening of the quadrupole doublet (data not shown), confirming the formation of the Mn^{IV}/Fe^{III}−R2 complex as the ultimate product also in the reaction of the fully reduced protein with H_2O_2.

Kinetics and Mechanism of the Reaction of the Mn^{II}/Fe^{II}−R2 Complex with H_2O_2. The expectation that this conversion proceeds by two sequential reactions with H_2O_2 via Mn^{III}/Fe^{III}−R2 and Mn^{IV}/Fe^{IV}−R2 intermediates was confirmed by stopped-flow absorption (spectra of selected reaction times are shown in Figure S3) and freeze-quench EPR experiments. A_{390}-versus-time traces from the reaction exhibit two resolved development phases followed by a slower decay phase (Figure 2B). Both development phases exhibit an approximately first-order dependence on H_2O_2 concentration (inset of Figure 2B). The plot of k_{obs} for the slower of the two phases versus H_2O_2 concentration (blue circles) gives a second-order rate constant (8 ± 1 M^{-1} s^{-1}) for combination with H_2O_2 that is indistinguishable from the value determined for the reaction of the Mn^{III}/Fe^{III}−R2 complex with H_2O_2. Values of k_{obs} for the decay phase are also indistinguishable from those for the decay phase in the reaction of the Mn^{III}/Fe^{III}−R2 complex at equivalent concentrations of H_2O_2 (not shown). Thus, the slower development phase and the decay phase reflect conversion of the Mn^{III}/Fe^{III}−R2 complex to the Mn^{IV}/Fe^{IV}−R2 complex (development) and then to the Mn^{IV}/Fe^{III}−R2 complex (the decay). The more rapid development phase corresponds to conversion of the Mn^{II}/Fe^{II}−R2 complex to the Mn^{III}/Fe^{III}−R2 complex by the first reaction with H_2O_2. The second-order rate constant for this step, 1.7 ± 0.3 mM^{-1} s^1 [from the inset of Figure 2B (gray diamonds)], is ~200 times that for the second H_2O_2-mediated cluster oxidation and similar to the rate constant for conversion of fully reduced ($Fe_2^{II/II}$) *Ec* R2 to met-R2 by H_2O_2 [6 ± 1 mM^{-1} s^{-1} (W. Jiang, C. Krebs, and J. M. Bollinger, Jr., unpublished data)].

EPR spectra of samples freeze-quenched during the reaction provide additional evidence for sequential accumulation of Mn^{III}/Fe^{III}−R2 and Mn^{IV}/Fe^{IV}−R2 intermediates (Figure 4). The spectral features of the first intermediate are broad[2] and thus neither as intense nor as easily quantifiable as the features of the Mn^{IV}/Fe^{IV}−R2 intermediate. Nevertheless, these features can readily be discerned (arrows in Figure 4) at shorter reaction times (e.g., 0.090 and 1.5 s) in the regions outside the sharp six-line spectrum of the Mn^{IV}/Fe^{IV}−R2 complex and can be seen to decay at longer times (13 s). The much sharper and more well-defined features of the Mn^{IV}/Fe^{IV}−R2 complex become apparent even early in the reaction but increase and become predominant at longer reaction times (13 s). Thus, the kinetics reflected in the EPR spectra are qualitatively consistent with the sequential formation of Mn^{III}/Fe^{III}−R2 and Mn^{IV}/Fe^{IV}−R2 intermediates on the pathway to the active Mn^{IV}/Fe^{III}−R2 product.

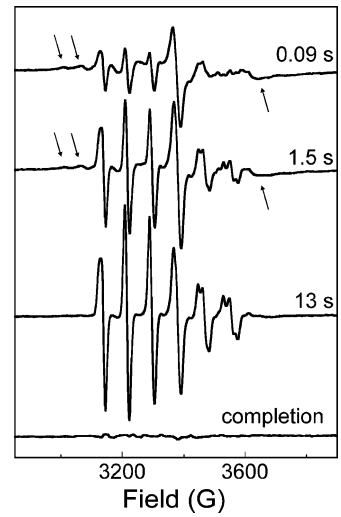

FIGURE 4: X-Band EPR spectra at 14.0 ± 0.2 K of freeze-quenched samples from the reaction of the Mn^{II}/Fe^{II}−R2 complex and H_2O_2. The reaction was initiated by mixing the Mn^{II}/Fe^{II}−R2 complex (0.90 mM R2 monomer, 0.5 equiv of Fe^{II}, and 1.0 equiv of Mn^{II}) with 0.5 equivalent volume of 45 mM H_2O_2, and samples were rapidly frozen at the indicated reaction times. For the spectra of the three freeze-quenched samples that are shown (indicated by reaction time), the spectrum of the reactant sample was scaled appropriately and then subtracted from the experimental spectra to resolve the contributions of the Mn^{III}/Fe^{III}−R2 and Mn^{IV}/Fe^{IV}−R2 intermediates. The arrows in the spectra of 0.09 and 1.5 s samples indicate features of the Mn^{III}/Fe^{III}−R2 intermediate. Spectrometer conditions were as follows: microwave frequency, 9.45 GHz; microwave power, 200 μW; modulation frequency, 100 kHz; modulation amplitude, 10 G; scan time, 167 s; time constant, 167 ms.

Reaction of the $Fe_2^{III/III}$−R2 Species with H_2O_2 Monitored by Stopped-Flow Absorption Spectroscopy. The demonstration described above that the Mn^{III}/Fe^{III} form of *Ct* R2 readily reacts with H_2O_2 contrasts with previous reports of very slow and inefficient conversion of the cognate ($Fe_2^{III/III}$ or met) form of *Ec* R2 to the active, $Fe_2^{III/III}/Y^{\bullet}$ state (*20*). To assess whether (i) the substitution of the metal ion, (ii) additional, more subtle structural differences between the active sites of the *Ct* and *Ec* R2 proteins, or (iii) some combination of these factors is primarily responsible for the greater reactivity of the *Ct* protein, the reaction of the homobinuclear $Fe_2^{III/III}$ form of *Ct* R2 with H_2O_2 was examined by stopped-flow absorption spectroscopy. Development of absorption is much (~10-fold) slower in this reaction than in the reaction of the Mn^{III}/Fe^{III} protein (Figure S4). The conclusion that the $Fe_2^{III/III}$ form reacts sluggishly was verified by directly monitoring decomposition of H_2O_2 in the presence of the apo, Mn^{IV}/Fe^{III}, $Fe_2^{III/III}$, and Mn^{III}/Fe^{III} forms of *Ct* R2. As illustrated in Figure S5, all four forms accelerate decay of H_2O_2 to some extent. However, only for the Mn^{III}/Fe^{III} form is there an obvious, stoichimetric "burst" of H_2O_2 decomposition. These results establish that substitution of the Fe^{III} with Mn^{III} is important, if not primarily determinant, in the greater H_2O_2 reactivity of the III/III oxidation state of the *Ct* R2 protein compared to *Ec* R2.

[3] The spectrum is published again here for comparison to the spectra of the R2 sample converted to the Mn^{IV}/Fe^{III} state by H_2O_2.

Scheme 1: Interconversions of Oxidation States of the Mn/Fe Cluster in *C. trachomatis* R2

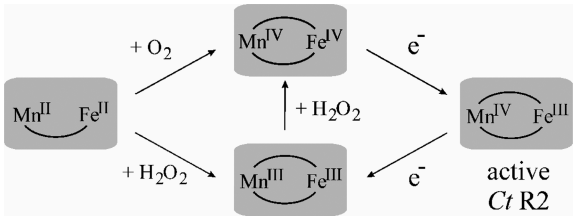

DISCUSSION

Scheme 1 summarizes the demonstrated redox interconversions of the *Ct* R2 Mn/Fe cofactor. In considering the potential relevance of the conversions mediated by H_2O_2 to the evolution and function of the novel cofactor, it is important to note that H_2O_2 is but one of several RO(N)S generated by the host's innate immune response. Others, including nitric oxide (NO•), superoxide, and peroxynitrite, are in some respects more reactive and seemingly more likely to target a bacterium's RNR. Indeed, NO• (*25, 26, 28, 29*), superoxide (*27*), and peroxynitrite (*30*) have been reported to target the Y•s of conventional class I RNRs, but we are not aware of any report that H_2O_2 does so. Nevertheless, a plausible mechanism by which H_2O_2 might inhibit a conventional class I RNR can be formulated from published data. As previously noted, it is known that regeneration of the Y• by in situ reduction of the $Fe_2^{III/III}$ cluster to $Fe_2^{II/II}$ and reaction of O_2 with the fully reduced cluster occurs in *E. coli* (*18, 19*) and probably also in other organisms. The presence of H_2O_2 would lead to a partition of the $Fe_2^{II/II}$ form between conversion to active R2 (by O_2) and conversion to met-R2 (by H_2O_2). For the case of the *Ec* protein, the rate constant for reaction of the fully reduced protein with O_2 is only ~50 times greater than the rate constant for its reaction with H_2O_2. Thus, H_2O_2 in the millimolar concentration range should be capable of competing effectively with ambient O_2 in aerobically growing cells for reaction with the $Fe_2^{II/II}$−R2 complex. The resulting conversion to met-R2 would delay reactivation by requiring (at least) another round of cluster reduction. Reaction of the met form with H_2O_2 to regenerate the active state directly, without the need for cluster reduction, is so inefficient *in vitro* (*20*) that it is not expected to be important *in vivo*. By contrast, trapping of the Mn^{II}/Fe^{II} form of *Ct* R2 by H_2O_2 gives a form, Mn^{III}/Fe^{III}−R2, that reacts efficiently with H_2O_2 to generate the active form. Thus, if inhibition of the ancestral form of the class Ic RNR (which might have been a $Fe_2^{III/III}$-containing enzyme) by H_2O_2 was an important defense mechanism for the ancestral host, then the advent of the Mn/Fe cofactor could have conferred a selective advantage to the mutant bacterium.

The structural changes to R2 (and perhaps also to R1) that might have been needed for this evolutionary "metal makeover" (*34*) remain to be defined. Likewise, there may be multiple contributors to the relatively high H_2O_2 reactivity of the *Ct* R2 cofactor in its III/III oxidation state. However, the comparatively meager H_2O_2 reactivity of the corresponding homobinuclear (diiron) cluster form implies that the metal substitution itself is crucial to the enhanced H_2O_2 reactivity. What additional enhanced, diminished, or novel reactivities toward RO(N)S might be conferred by the metal substitution remain to be established and may shed more light on the evolution of the cofactor.

SUPPORTING INFORMATION AVAILABLE

A 4.2 K/53 mT Mössbauer spectrum of a sample prepared by treating the Mn^{IV}/Fe^{III}−R2 complex with 1.2 equiv of dithionite, selected time-dependent UV−visible absorption spectra from the reactions of the Mn^{II}/Fe^{II}−R2 and Mn^{III}/Fe^{III}−R2 species with H_2O_2, absorbance-versus-time traces from the reaction of the $Fe_2^{III/III}$−R2 complex with H_2O_2, and kinetics of the decomposition of H_2O_2 by various forms of R2. This material is available free of charge via the Internet at http://pubs.acs.org.

REFERENCES

1. Stubbe, J. (2003) Di-iron-tyrosyl radical ribonucleotide reductases. *Curr. Opin. Chem. Biol. 7*, 183–188.
2. Bollinger, J. M., Jr., Edmondson, D. E., Huynh, B. H., Filley, J., Norton, J. R., and Stubbe, J. (1991) Mechanism of assembly of the tyrosyl radical-dinuclear iron cluster cofactor of ribonucleotide reductase. *Science 253*, 292–298.
3. Ravi, N., Bollinger, J. M., Jr., Huynh, B. H., Edmondson, D. E., and Stubbe, J. (1994) Mechanism of Assembly of the Tyrosyl Radical-Diiron(III) Cofactor of *E. coli* Ribonucleotide Reductase: 1. Mössbauer Characterization of the Diferric Radical Precursor. *J. Am. Chem. Soc. 116*, 8007–8014.
4. Sturgeon, B. E., Burdi, D., Chen, S., Huynh, B. H., Edmondson, D. E., Stubbe, J., and Hoffman, B. M. (1996) Reconsideration of **X**, the diiron intermediate formed during cofactor assembly in *E. coli* ribonucleotide reductase. *J. Am. Chem. Soc. 118*, 7551–7557.
5. Stubbe, J., Nocera, D. G., Yee, C. S., and Chang, M. C. Y. (2003) Radical initiation in the class I ribonucleotide reductase: Long-range proton-coupled electron transfer? *Chem. Rev. 103*, 2167–2202.
6. Nordlund, P., and Reichard, P. (2006) Ribonucleotide reductases. *Annu. Rev. Biochem. 75*, 681–706.
7. Licht, S., Gerfen, G. J., and Stubbe, J. (1996) Thiyl radicals in ribonucleotide reductases. *Science 271*, 477–481.
8. Mao, S. S., Yu, G. X., Chalfoun, D., and Stubbe, J. (1992) Characterization of C439SR1, a mutant of *Escherichia coli* ribonucleotide diphosphate reductase: Evidence that C439 is a residue essential for nucleotide reduction and that C439SR1 is a protein possessing novel thioredoxin-like activity. *Biochemistry 31*, 9752–9759.
9. Baker, C. H., Banzon, J., Bollinger, J. M., Jr., Stubbe, J., Samano, V., Robins, M. J., Lippert, B., Jarvi, E., and Resvick, R. (1991) 2′-Deoxy-2′-methylenecytidine and 2′-deoxy-2′,2′-difluorocytidine 5′-diphosphates: Potent mechanism-based inhibitors of ribonucleotide reductase. *J. Med. Chem. 34*, 1879–1884.
10. Lori, F., Malykh, A., Cara, A., Sun, D., Weinstein, J. N., Lisziewicz, J., and Gallo, R. C. (1994) Hydroxyurea as an inhibitor of human immunodeficiency virus-type 1 replication. *Science 266*, 801–805.
11. Mayhew, C. N., Phillips, J. D., Greenberg, R. N., Birch, N. J., Elford, H. L., and Gallicchio, V. S. (1999) *In vivo* and *in vitro* comparison of the short-term hematopoietic toxicity between hydroxyurea and trimidox or didox, novel ribonucleotide reductase inhibitors with potential anti-HIV-1 activity. *Stem Cells 17*, 345–356.
12. Ehrenberg, A., and Reichard, P. (1972) Electron spin resonance of the iron-containing protein B2 from ribonucleotide reductase. *J. Biol. Chem. 247*, 3485–3488.
13. Sartorelli, A. C., Agrawal, K. C., and Moore, E. C. (1978) 5-Amino-1-formylisoquinoline thiosemicarbazone, an inhibitor of ribonucleotide reductase. *Nucleic Acid Chem. 2*, 945–954.
14. van der Donk, W. A., Yu, G., Perez, L., Sanchez, R. J., Stubbe, J., Samano, V., and Robins, M. J. (1998) Detection of a New Substrate-Derived Radical during Inactivation of Ribonucleotide Reductase from *Escherichia coli* by Gemcitabine 5′-Diphosphate. *Biochemistry 37*, 6419–6426.
15. Lam, K. Y., Fortier, D. G., Thomson, J. B., and Sykes, A. G. (1990) Kinetics of inactivation of the tyrosine radical of the B2 subunit of *E. coli* ribonucleotide reductase. *J. Chem. Soc., Chem. Commun.*, 658–660.

16. Lassmann, G., Thelander, L., and Gräslund, A. (1992) EPR stopped-flow studies of the reaction of the tyrosyl radical of protein R2 from ribonucleotide reductase with hydroxyurea. *Biochem. Biophys. Res. Commun. 188*, 879–887.
17. Fontecave, M., Eliasson, R., and Reichard, P. (1987) NAD(P)H: flavin oxidoreductase of *Escherichia coli*. A ferric iron reductase participating in the generation of the free radical of ribonucleotide reductase. *J. Biol. Chem. 262*, 12325–12331.
18. Fontecave, M., Eliasson, R., and Reichard, P. (1989) Enzymic regulation of the radical content of the small subunit of *Escherichia coli* ribonucleotide reductase involving reduction of its redox centers. *J. Biol. Chem. 264*, 9164–9170.
19. Wu, C.-H., Jiang, W., Krebs, C., and Stubbe, J. (2007) YfaE, a Ferredoxin Involved in Diferric-Tyrosyl Radical Maintenance in *Escherichia coli* Ribonucleotide Reductase. *Biochemistry 46*, 11577–11588.
20. Sahlin, M., Sjöberg, B. M., Backes, G., Loehr, T., and Sanders-Loehr, J. (1990) Activation of the iron-containing B2 protein of ribonucleotide reductase by hydrogen peroxide. *Biochem. Biophys. Res. Commun. 167*, 813–818.
21. Roshick, C., Iliffe-Lee, E. R., and McClarty, G. (2000) Cloning and Characterization of Ribonucleotide Reductase from *Chlamydia trachomatis*. *J. Biol. Chem. 275*, 38111–38119.
22. Högbom, M., Stenmark, P., Voevodskaya, N., McClarty, G., Gräslund, A., and Nordlund, P. (2004) The radical site in Chlamydial ribonucleotide reductase defines a new R2 subclass. *Science 305*, 245–248.
23. Voevodskaya, N., Lendzian, F., and Gräslund, A. (2005) A stable Fe^{III}-Fe^{IV} replacement of tyrosyl radical in a class I ribonucleotide reductase. *Biochem. Biophys. Res. Commun. 330*, 1213–1216.
24. Voevodskaya, N., Narvaez, A. J., Domkin, V., Torrents, E., Thelander, L., and Gräslund, A. (2006) Chlamydial ribonucleotide reductase: Tyrosyl radical function in catalysis replaced by the Fe^{III}-Fe^{IV} cluster. *Proc. Natl. Acad. Sci. U.S.A. 103*, 9850–9854.
25. Lepoivre, M., Fieschi, F., Coves, J., Thelander, L., and Fontecave, M. (1991) Inactivation of ribonucleotide reductase by nitric oxide. *Biochem. Biophys. Res. Commun. 179*, 442–448.
26. Roy, B., Lepoivre, M., Henry, Y., and Fontecave, M. (1995) Inhibition of Ribonucleotide Reductase by Nitric Oxide Derived from Thionitrites: Reversible Modifications of Both Subunits. *Biochemistry 34*, 5411–5418.
27. Gaudu, P., Niviere, V., Petillot, Y., Kauppi, B., and Fontecave, M. (1996) The irreversible inactivation of ribonucleotide reductase from *Escherichia coli* by superoxide radicals. *FEBS Lett. 387*, 137–140.
28. Guittet, O., Ducastel, B., Salem, J. S., Henry, Y., Rubin, H., Lemaire, G., and Lepoivre, M. (1998) Differential sensitivity of the tyrosyl radical of mouse ribonucleotide reductase to nitric oxide and peroxynitrite. *J. Biol. Chem. 273*, 22136–22144.
29. Guittet, O., Roy, B., and Lepoivre, M. (1999) Nitric oxide. A radical molecule in quest of free radicals in proteins. *Cell. Mol. Life Sci. 55*, 1054–1067.
30. Guittet, O., Decottignies, P., Serani, L., Henry, Y., Le Marechal, P., Laprevote, O., and Lepoivre, M. (2000) Peroxynitrite-Mediated Nitration of the Stable Free Radical Tyrosine Residue of the Ribonucleotide Reductase Small Subunit. *Biochemistry 39*, 4640–4648.
31. Jiang, W., Yun, D., Saleh, L., Barr, E. W., Xing, G., Hoffart, L. M., Maslak, M.-A., Krebs, C., and Bollinger, J. M., Jr. (2007) A Manganese(IV)/Iron(III) Cofactor in *Chlamydia trachomatis* Ribonucleotide Reductase. *Science 316*, 1188–1191.
32. Jiang, W., Bollinger, J. M., Jr., and Krebs, C. (2007) The active form of *Chlamydia trachomatis* ribonucleotide reductase R2 protein contains a heterodinuclear Mn(IV)/Fe(III) cluster with $S = 1$ ground state. *J. Am. Chem. Soc. 129*, 7504–7505.
33. Jiang, W., Hoffart, L. M., Krebs, C., and Bollinger, J. M., Jr. (2007) A Mn(IV)/Fe(IV) Intermediate in Assembly of the Mn(IV)/Fe(III) Cofactor of *Chlamydia trachomatis* Ribonucleotide Reductase. *Biochemistry 46*, 8709–8716.
34. Yarnell, A. (2007) Enzyme gets Metal Makeover. *Chem. Eng. News 85* (22), 31.
35. Hassan, H. M., and Schrum, L. W. (1994) Roles of manganese and iron in the regulation of the biosynthesis of manganese-superoxide dismutase in *Escherichia coli*. *FEMS Microbiol. Rev. 14*, 315–323.
36. Daly, M. J., Gaidamakova, E. K., Matrosova, V. Y., Vasilenko, A., Zhai, M., Leapman, R. D., Lai, B., Ravel, B., Li, S.-M. W., Kemner, K. M., and Fredrickson, J. K. (2007) Protein oxidation implicated as the primary determinant of bacterial radioresistance. *PLoS Biol. 5*, 769–779.
37. Grass, G., Franke, S., Taudte, N., Nies, D. H., Kucharski, L. M., Maguire, M. E., and Rensing, C. (2005) The Metal Permease ZupT from *Escherichia coli* Is a Transporter with a Broad Substrate Spectrum. *J. Bacteriol. 187*, 1604–1611.
38. Clifford, D. P., and Repine, J. E. (1982) Hydrogen peroxide-mediated killing of bacteria. *Mol. Cell. Biochem. 49*, 143–149.
39. Gerez, C., and Fontecave, M. (1992) Reduction of the small subunit of *Escherichia coli* ribonucleotide reductase by hydrazines and hydroxylamines. *Biochemistry 31*, 780–786.
40. Krebs, C., Chen, S., Baldwin, J., Ley, B. A., Patel, U., Edmondson, D. E., Huynh, B. H., and Bollinger, J. M., Jr. (2000) Mechanism of Rapid Electron Transfer during Oxygen Activation in the R2 Subunit of *Escherichia coli* Ribonucleotide Reductase. 2. Evidence for and Consequences of Blocked Electron Transfer in the W48F Variant. *J. Am. Chem. Soc. 122*, 12207–12219.
41. Price, J. C., Barr, E. W., Tirupati, B., Bollinger, J. M., Jr., and Krebs, C. (2003) The First Direct Characterization of a High-Valent Iron Intermediate in the Reaction of an α-Ketoglutarate-Dependent Dioxygenase: A High-Spin Fe(IV) Complex in Taurine/α-Ketoglutarate Dioxygenase (TauD) from *Escherichia coli*. *Biochemistry 42*, 7497–7508.
42. Jameson, G. N. L., Jin, W., Krebs, C., Pereira, A. S., Tavares, P., Liu, X., Theil, E. C., and Huynh, B. H. (2002) Stoichiometric Production of Hydrogen Peroxide and Parallel Formation of Ferric Multimers through Decay of the Diferric-Peroxo Complex, the First Detectable Intermediate in Ferritin Mineralization. *Biochemistry 41*, 13435–13443.
43. Münck, E. (2000) Aspects of ^{57}Fe Mössbauer spectroscopy, in *Physical Methods in Bioinorganic Chemistry* (Que, L., Jr., Ed.) pp 287–319, University Science Books, Sausalito, CA.

BI702085Z